RESEARCH ARTICLE

AC Loss in REBCO Coil Windings Wound With Various Cables: Effect of Current Distribution Among the Cable Strands

WENJUAN SONG [1], (Member, IEEE), **RODNEY A. BADCOCK** [2], (Senior Member, IEEE),
NICHOLAS J. LONG [2], (Senior Member, IEEE), AND **ZHENAN JIANG** [2], (Senior Member, IEEE)

[1] James Watt School of Engineering, University of Glasgow, G12 8QQ Glasgow, U.K.
[2] Robinson Research Institute, Victoria University of Wellington, Lower Hutt 5046, New Zealand

Corresponding authors: Wenjuan Song (wenjuan.song@glasgow.ac.uk) and Zhenan Jiang (zhenan.jiang@vuw.ac.nz)

ABSTRACT To construct large-scale superconducting devices, it is critical to enhance the current carrying capability of superconducting coils. One practical approach is to utilise assembled cables, composed of multiple strands, for the winding. There have only been a few investigations of the dependence of current distribution among the strands on the AC losses of the cables and coils wound with these cables. In this work, we studied three types of cables; 1) 8/2 (eight 2 mm-wide strands) Roebel cable, 8/2 Roebel; 2) two parallel stacks (TPS) which have the same geometrical dimensions as the Roebel cable, 8/2 TPS; and 3) an equivalent four-conductor stack (ES) comprising four 4 mm-wide conductors, 4/4 ES. We proposed a new numerical approach that can achieve equal current sharing and free current sharing among the strands. We examined the loss behaviour of all three types of straight cables and two coil assemblies comprising two, and eight, stacks of double pancakes (DPCs) wound with these cables, respectively. 2D FEM analysis was carried out in COMSOL Multiphysics using the H – formulation. The stacks were modelled in parallel connection, with the same electric field applied to all strands, so that current is distributed between the conductors. Simulated transport AC loss results in the straight 8/2 Roebel cable, 8/2 TPS and 4/4 ES were compared with previously measured results as well as each other. The numerical AC loss results in two coil windings 2-DPC and 8-DPC wound with the 8/2 Roebel cables were compared with the results in coil windings wound with the 8/2 TPS and 4/4 ES. No transposition was introduced at the connection between double pancakes, in order that current can be shared among the strands in the 8/2 TPS and 4/4 ES. The results indicate that AC loss in the straight 8/2 TPS and 4/4 ES is larger than that in the 8/2 Roebel cable. Current is more concentrated in the outer strands for the straight 8/2 TPS and 4/4 ES than the 8/2 Roebel cable and causes greater AC loss than the 8/2 Roebel cable. The 8-DPC coil winding wound with the 8/2 Roebel cable has the smallest loss and the coil winding wound with the 8/2 TPS has the greatest loss at two current amplitudes investigated. At 113 A, the AC loss value in the 8-DPC coil winding wound with the 8/2 TPS is 2.2 times of that wound with the 8/2 Roebel cable.

INDEX TERMS Current sharing, coil windings, Roebel cable, parallel stack, current distribution.

I. INTRODUCTION

Large scale high temperature superconducting (HTS) power applications present promising solutions for the electrical

The associate editor coordinating the review of this manuscript and approving it for publication was Su Yan.

systems within the transportation and energy sectors. Thanks to the remarkable capabilities enabled by HTS technology, HTS applications encompass high efficiency and power density, compact size, and lightweight design, etc. Many R&D projects and studies have been carried out on superconducting applications in the transportation and

energy sectors, including superconducting transformers [1], [2], [3], [4], power transmission cables [5], [6], rotating machines [7], [8], fault current limiters [9], [10], Superconducting Magnetic Energy Storage (SMES) [11], [12], magnets [13], [14], etc. The integration of HTS-based devices in these sectors and systems enables us to tackle decarbonation and energy challenges more effectively and efficiently.

To achieve high power rating and high-power density, it is essential for the HTS devices to be wound with superconducting cables comprised of multiple tapes to carry high current [15], [16]. One example of increasing current-carrying capability is Roebel cable, which is a fully transposed cable assembled by multiple punched ReBCO strands [15], [17], [18], [19], [20]. Another technique is to assemble ReBCO tapes into a simply stacked cable with or without transposition of the tapes [21], [22], [23], [24], [25]. In a transposed cable, the current in each strand is equally distributed. Whereas, in a simple stack without transposition, current distributes unevenly in each tape/strand, for example, with greater current flowing in outer tapes and less current in the inner tapes [26], [27], [28]. This leads to an undesirable AC loss from the cables. In a coil winding wound with a simple stack, the unequal current sharing between the tapes will be more severe due to the difference in inductance for each tape and hence leads to large AC loss in the coil winding [29]. It is important to note that these losses are closely linked with the device efficiency and lead to a thermal load that must be removed by the cooling systems, which has a high cooling penalty [30]. Thus, for high current AC applications, the unequal current sharing between the tapes in an assembled cable is a critical issue concerning losses that must be studied and solved.

In our previous research, we explored the impact of unequal current distribution in non-inductive bifilar coils, wound with Roebel cable and simple stacks, for superconducting fault current limiter [31]. We experimentally compared the measured transport AC losses of Roebel cables and simple stacks with, and without, transposition. However, there is limited work published on the AC loss in superconducting inductive coil windings comprised of double pancake coils wound with transposed, and non-transposed, cables and the impact of unequal current sharing on AC loss in the coil windings.

In this work, three types of cables are studied; i) 8/2 (eight 2 mm-wide strands) Roebel cable, 8/2 Roebel; ii) two parallel stack which have the same geometrical dimensions as the Roebel cable, 8/2 TPS; iii) an equivalent four-conductor stack comprising four 4 mm-wide conductors, 4/4 ES. Figure 1(a) shows the schematic of the three cables. Firstly, the simulated transport AC loss results in the straight 8/2 Roebel cable were compared with measured results as well as 8/2 TPS and 4/4 ES. Next, we evaluated the loss behaviour of two coil windings comprising two, and eight stacks of double pancakes (DPCs) wound with these cables, respectively. The numerical AC loss results in the two coil windings wound with the 8/2 Roebel cables were compared with

the results in the coil windings wound with 8/2 TPS and 4/4 ES.

This paper is structured as follows. Section I introduces the importance and motivation of the work. Section II explains the numerical methods and specifications of the studied cables. Section III validates the numerical model through comparison with experimental results. Section IV shows the results and the analysis of straight 8/2 Roebel cable, 8/2 TPS and 4/4 ES. Section V reports the results and the analysis on superconducting coils wound with the 8/2 Roebel, 8/2 TPS and 4/4 ES. Conclusion is presented in section VI.

II. NUMERICAL APPROACHES
A. SIMULATION FOR STRAIGHT CONDUCTOR AND COILS
A two-dimensional (2D) FEM model employing H-formulation was built in COMSOL to study the AC loss characteristics of the straight 8/2 Roebel cable, 8/2 TPS, 4/4 ES, as well as stacks of coil windings wound with the three cables [32], [33], [34], [35]. Two state variables were implemented, $\boldsymbol{H} = [H_x, H_y]^T$, where H_x and H_y are magnetic fields parallel and perpendicular to the tape wide-surface. A power law relation was used to represent the highly nonlinear relationship of local electric field E and local current density J in the HTS layer:

$$E/J = \left(E_0/J_c\left(\boldsymbol{B}\right)\right)\left(|J/J_c\left(\boldsymbol{B}\right)|\right)^{n-1} \quad (1)$$

where $E_0 = 1\ \mu\text{V/cm}$, $n = 30$ is the power index derived from V-I characteristic; $J_c(\boldsymbol{B})$ is the critical current density dependence on local magnetic field and lateral position. In this work, a modified Kim model was adopted for $J_c(\boldsymbol{B})$ profile, as expressed in (2). k, α, and B_0 are curve fitting parameters and the values used in this study are 0.3, 0.7, and 42.6 mT, respectively.

$$J_c\left(\boldsymbol{B}\right) = J_{c0}\left(1 + \left(k^2 B_\parallel^2 + B_\perp^2\right)\bigg/B_0^2\right)^{-\alpha} \quad (2)$$

The governing equation (3) is derived by combining Faraday's law, Ampere's law, Ohm's law, and constitutive law. Equation (4) is obtained by substituting H_x and H_y into (3). μ_0 is the magnetic permeability of the free space. μ_r is the relative magnetic permeability. Here, $\mu_r = 1$ holds true for all the cases studied in this work.

$$\partial(\mu_0\mu_r\boldsymbol{H})/\partial t + \nabla\times(\rho\nabla\times\boldsymbol{H}) = 0 \quad (3)$$

$$\begin{cases} \mu_0\mu_r\dfrac{\partial H_x}{\partial t} + \dfrac{\partial\left(\rho\left(\frac{\partial H_y}{\partial x} - \frac{\partial H_x}{\partial y}\right)\right)}{\partial y} = 0 \\[2ex] \mu_0\mu_r\dfrac{\partial H_y}{\partial t} - \dfrac{\partial\left(\rho\left(\frac{\partial H_y}{\partial x} - \frac{\partial H_x}{\partial y}\right)\right)}{\partial x} = 0 \end{cases} \quad (4)$$

For simplification, 2D axisymmetric model was employed to simulate the electromagnetic behavior in coil windings, with two state variables $\boldsymbol{H} = [H_r, H_z]^T$ [36]. The governing
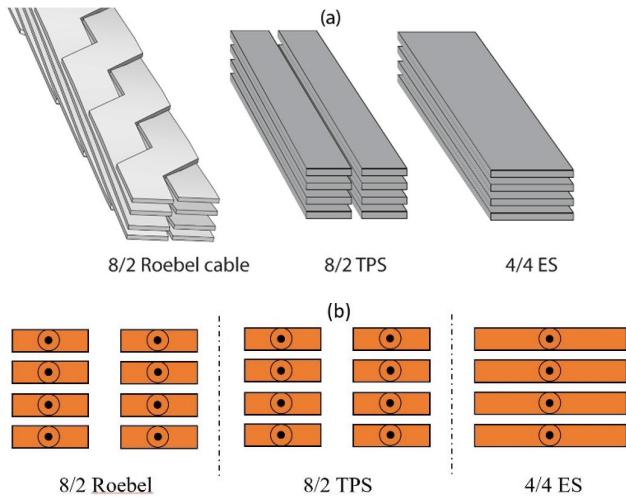
FIGURE 1. (a) Schematic of the three studied cables (b) Cross-section of the three cables.

TABLE 1. Specifications of different cables.

Items	8/2 ROEBEL	8/2 TPS	4/4 ES
Total strand number	8	8	4
Strand number per layer	2	2	1
Layer number per cable	4	4	4
Width of the cable, mm	5	5	4
Width of each strand, mm	2	2	4
Thickness of each strand, mm	0.1	0.1	0.1

equation is shown in (5),

$$\begin{cases} \mu_0\mu_r\dfrac{\partial H_r}{\partial t} - \dfrac{1}{r}\dfrac{\partial\left(r\rho\left(\frac{\partial H_r}{\partial z}-\frac{\partial H_z}{\partial r}\right)\right)}{\partial z} = 0 \\[4mm] \mu_0\mu_r\dfrac{\partial H_z}{\partial t} + \dfrac{1}{r}\dfrac{\partial\left(r\rho\left(\frac{\partial H_r}{\partial z}-\frac{\partial H_z}{\partial r}\right)\right)}{\partial r} = 0 \end{cases} \quad (5)$$

B. MODEL SETUP FOR THE THREE STUDIED CABLES AND THE COILS WOUND BY THEM

Figure 1(b) shows the schematic of the studied cables' cross-sections. Equal current flows in each strand in the 8/2 Roebel cable; 8/2 TPS has the same geometry as the 8/2 Roebel cable but allows free current distribution among the strands; 4/4 ES has the identical valid conductor cross-section area with 8/2 Roebel cable and 8/2 TPS, but allows free current distribution among the strands. It is worthy to note that previous reports concluded that Roebel cables can be treated as two parallel stacks carrying equal current in each strand [16], [17], [18]. Table 1 lists the specifications of the cables.

Figure 2 illustrates the modelled cross-sections of the three cables and the symmetry boundary conditions applied in COMSOL software. Figure 2(a) represents the modelling of 8/2 Roebel cable and 8/2 TPS since they share the same cross-section, while Figure 2(b) simulates the 4/4 ES. Due to the symmetry, only a quarter model is simulated to reduce computing time. To consider the symmetry, $H_x = 0$ is applied on x-axis, and $H_y = 0$ is applied on y-axis.

Two coil windings wound with these three cables, namely 8/2 Roebel, 8/2 TPS, and 8/2 ES, were investigated, including
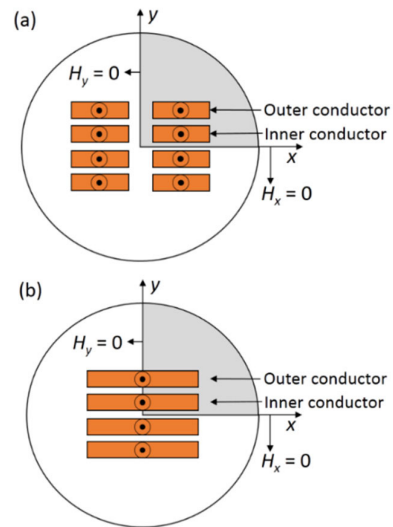

FIGURE 2. Schematic of the numerical model for the three studied cable (a) 8/2 Roebel cable and 8/2 TPS (b) 4/4 ES (only a quarter model was simulated considering symmetry).

TABLE 2. Specifications of modelled coil windings.

Items	2-DPC	8-DPC
Inner diameter (mm)	60	60
No. of turns in radial direction	10	10
Winding thickness (mm)	4	4
Winding height, L (mm)	22	88
Gap between each PC in one DPC (mm)	0.2	0.2
Gap between DPCs (mm)	1	1

a coil winding comprised of a stack of two double pancake coils (2-DPC), and eight double pancake coils (8-DPC), respectively. Table 2 lists the specifications of the coil windings wound with the three cables.

Figures 3(a)-(c) show the schematic of current distribution in a 1-DPC wound with the 8/2 Roebel, 8/2 TPS and 4/4 ES. In figure 3(a), current is equally distributed in each strand of the 8/2 Roebel cable due to its fully – transposed nature. Pointwise constraint is applied in the partial differential equation (PDE) module for each strand. In figure 3(b), free current-sharing is defined in the 8/2 TPS cable, where the strand carrying the same amount of current is denoted using the same colour. This case is similar to the "coupled at end" case in [25]. The current-sharing pattern among all strands is repeated for each turn due to the structure of the coil winding. Similarly, in figure 3(c), free current-sharing is defined for the 4/4 ES cable. The different colour in each strand of the 4/4 ES denotes free current sharing. In a 1-DPC level, the current sharing pattern is linked and repeated for each turn for this case as well.

III. MODEL VERIFICATION

Figure 4 shows the simulated transport AC loss in the straight 8/2 Roebel cable at 59 Hz, plotted as a function of the Roebel cable current and compared with the measured AC losses of the cable [36]. In the figure, the theoretical transport AC losses estimated by Norris-ellipse (N-e) and Norris-strip
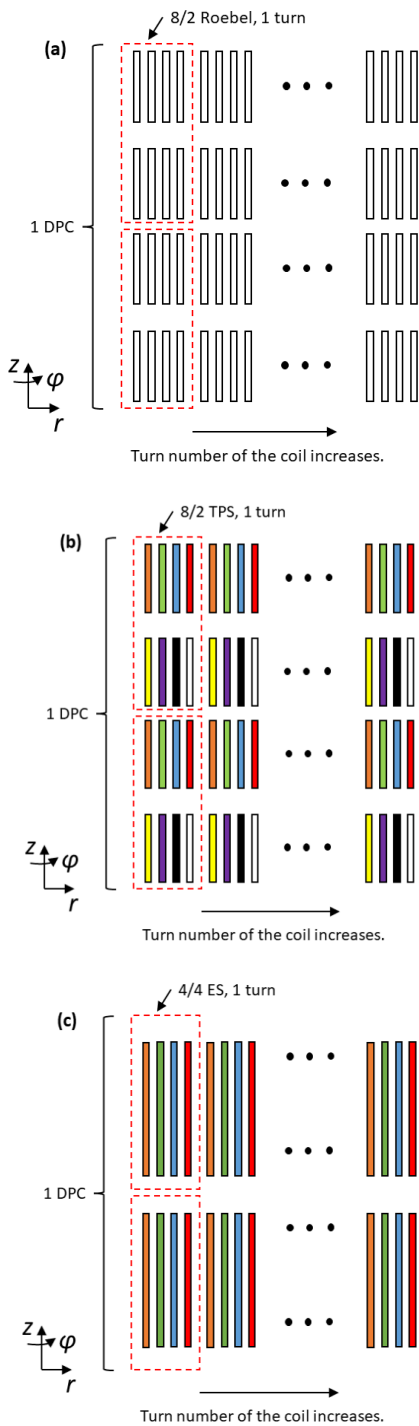
FIGURE 3. Schematic of a 1-DPC wound with the three cables (a) wound with the 8/2 Roebel cable, where equal current flowing in each strand (b) wound with 8/2 TPS, which has the same geometry as the 8/2 Roebel cable, but allowing free current distribution among strands (c) wound with 4/4 ES, which has the identical valid conductor cross-section area but allowing free current distribution among strands.

FIGURE 4. Comparison of measured and simulated AC loss values in the 8/2 Roebel cable.
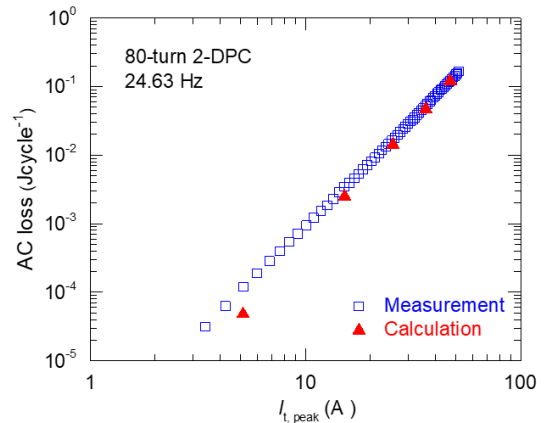
FIGURE 5. The simulated results for a 2-DPC coil winding agree with the measured AC loss results.

The simulated AC losses fall between N-e and N-s in the low current region and agrees well with N-s at high current amplitudes. The simulated losses of the 8/2 Roebel cable have a good agreement with the measured ones although slightly smaller.

Figure 5 shows the simulated AC loss in a 2-DPC coil winding compared with measured results. The modelling method for the coil is identical to what has been presented in Chapter II. The 2-DPC coil winding was wound with 4 mm – wide SuperPower wires. The measurement was carried out at 24.63 Hz. Calculation reasonably reproduces the measured values, and the results validate the simulation method for coil windings, which has been used to produce the results for 2-DPC and 8-DPC wound with the three cables in Chapter V.

IV. RESULTS ANALYSIS: STRAIGHT ROEBEL CABLE VS. STACKS

Figure 6 shows the simulated current distributions in the 'inner conductor' and 'outer conductor' of the 8/2 Roebel cable and 8/2 TPS defined in figure 1 at various $I_{t, turn}/I_{c0, cable}$ values when $\omega t = 3\pi/2$, where $I_{t, turn}$ is the total current amplitude for the 8/2 Roebel cable and 8/2 TPS. It is worth noting that 'inner conductor' and 'outer conductor' could represent the other three pairs of conductors in the 8/2 Roebel cable and 8/2 TPS due to the symmetry. The 'inner conductor' and 'outer conductor' carry exactly

(N-s) models using the measured cable I_c value 164 A are plotted together. The modelling method of the 8/2 Roebel is identical to what we described in Chapter II.
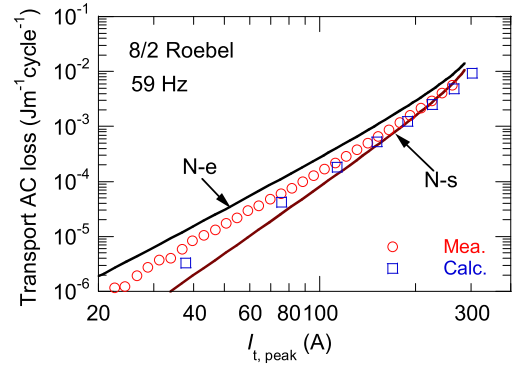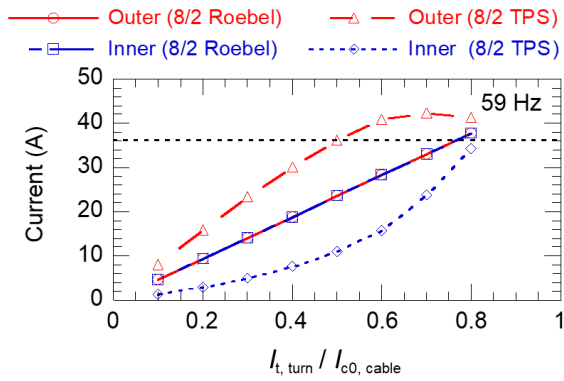
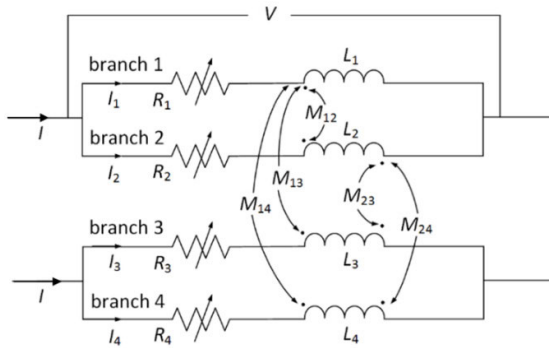**FIGURE 6.** Current distribution in the 8/2 Roebel cable and 8/2 TPS.

FIGURE 7. Schematic of magnetic field coupling among strands (only half of the cable is considered).

the same current for the whole current range in the 8/2 Roebel cable. In the 8/2 TPS, with increasing $I_{t, turn}$, current in both the 'inner conductor' and 'outer conductor' increases linearly only until $I_{t, turn}/I_{c0, cable}$ reaches 0.5. The 'inner conductor' in the 8/2 TPS carries much less current than the 'outer conductor' and the difference between the current values is the largest when $I_{t, turn}/I_{c0, cable}$ is around 0.5. The current in the 'outer conductor' in the 8/2 TPS saturates from $I_{t, turn}/I_{c0, cable}$ approximately 0.7 and becomes slightly smaller with increasing $I_{t, turn}$. On the other hand, current in the 'inner conductor' in the 8/2 TPS becomes larger more rapidly from $I_{t, turn}/I_{c0, cable} > 0.5$. This clearly indicates current redistribution between the two conductors through the terminals of the 8/2 TPS and the behaviour could be explained using a circuit model described in figure 7. At $I_{t, turn}/I_{c0, cable} = 0.3$ and 0.7, the current amplitudes of the 'surface conductor' and 'inner conductor' in the TPS are 4.97 A, 23.40 A, and 23.8 A, 42.38 A, respectively.

Considering symmetry, the circuit illustrates half cable, i. e. 4 strands in the 8/2 Roebel cable and 8/2 TPS: the 'outer conductor' and 'inner conductor' in the upper right half; the 'outer conductor' and 'inner conductor' in the bottom right half which carry current with the same direction as their upper counterpart conductors. Branch 1 refers to the upper 'outer conductor', branch 2 refers to the upper 'inner conductor', branch 3 refers to the bottom 'inner conductor', branch 4 refers to the bottom 'outer conductor'. Considering current direction in each conductor, the equations for the circuit for

the 'outer conductor' and 'inner conductor' can be written as follows,

$$V = (R_1 + j\omega L_1) I_1 + j\omega M_{12}I_2 + j\omega M_{13}I_3 + j\omega M_{14}I_4 \quad (6)$$

$$V = (R_2 + j\omega L_2) I_2 + j\omega M_{21}I_1 + j\omega M_{23}I_3 + j\omega M_{24}I_4 \quad (7)$$

where R_1 and R_2 are resistance values defined derived from the $E–J$ relationship of the conductors; L_1, L_2 are self-inductance values of the two conductors, I_1, I_2, I_3, and I_4 are current values in each branch; I is total current for the two branches; and M_{12}, M_{13}, M_{14}, M_{21}, M_{23}, M_{24} are the mutual inductance of branches defined as in figure 7. Due to the symmetry in the cable level, $I_1 + I_2 = I_3 + I_4$; $I_1 = I_4$ and $I_2 = I_3$; $M_{13} = M_{24}$. In addition, $L_1 = L_2 = L$ due to the same geometry and material of the conductors. Substituting the equivalent parameters in equations (6) and (7), we get the ratio of I_1/I_2,

$$\frac{I_1}{I_2} = \frac{R_2 + j\omega(L_2+M_{23} - M_{12} - M_{13})}{R_1 + j\omega(L_1+M_{14} - M_{21} - M_{24})} \quad (8)$$

When I is small, R_1 and R_2 are nearly zero; $L_2+M_{23} - M_{12} - M_{13}$ is bigger than $L_1+M_{14} - M_{21} - M_{24}$, since M_{23} is strong than M_{14}.

Figures 8(a) and (c) compare the current distribution J/J_c in the 8/2 Roebel cable and the 8/2 TPS at $I_t/I_{c0} = 0.8$, respectively. As shown in figure 8(a), we observe nearly the same pattern of J/J_c distribution in "Outer conductor" and "Inner conductor" at $I_t/I_{c0} = 0.8$, and both conductors are not yet fully penetrated, that both conductors have a portion of sub-critical area. In contrast, the pattern of J/J_c distribution in figure 8(c) is remarkably different. $|J/J_c|$ value of the "Outer conductor" in the 8/2 TPS is greater than 1 across the conductor width whereas there is 1/3 of the conductor width has less than 1 for the "Inner conductor".

Loss power density distribution in the 8/2 Roebel cable and the 8/2 TPS at $I_t/I_{c0} = 0.8$ are plotted and compared in figures 8(b) and (d). Both "Outer conductor" and "Inner conductor" have a portion of the conductor width that does not generate AC loss, as seen in figure 8(b), and this is aligned with the fact that both conductors have an area where $|J/J_c| < 1$. However, in figure 8(d), "Outer conductor" in the 8/2 TPS generates AC loss across the conductor width, and "Inner conductor" has a big area that does not generate AC loss at all due to the low J/J_c values in the area. This shows that each strand in the 8/2 Roebel cable behaves broadly equally in generating AC loss; whereas each strand in non-transposed cables behaves unequally in loss generation due to unequal current-sharing.

Figure 9 compares the transport AC loss values in the straight 8/2 Roebel cable, 8/2 TPS and 4/4 ES at 59 Hz. It is observed that for a given cable current, 4/4 ES has the greatest loss while Roebel cable has the smallest loss among the three cable types due to the equal current sharing as explained in figure 6 and figure 8. The difference in the AC loss values between the cables becomes greater with increasing the amplitude of the cable current.

At $I_{t, peak} = 151$ A and 302 A, AC loss in the 8/2 TPS is 1.06 times and 1.14 times of that in Roebel, respectively. AC loss values in the 8/2 TPS is smaller than 4/4 ES, due to
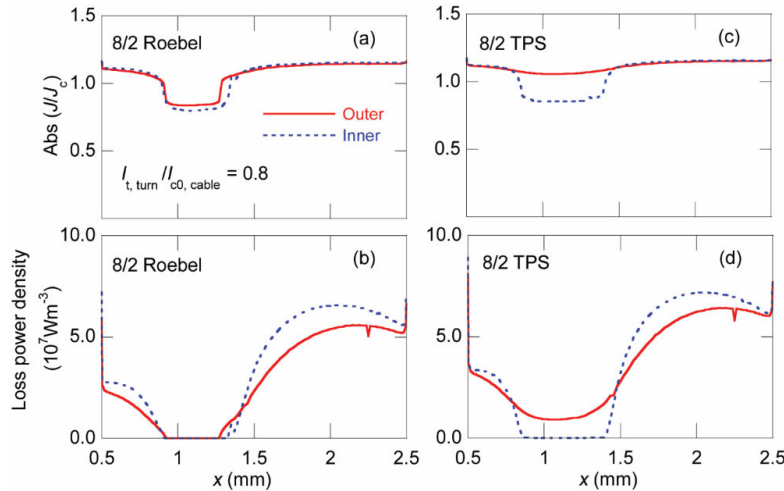
FIGURE 8. J/Jc distribution and loss power density distribution in the 8/2 Roebel cable and 8/2 TPS.
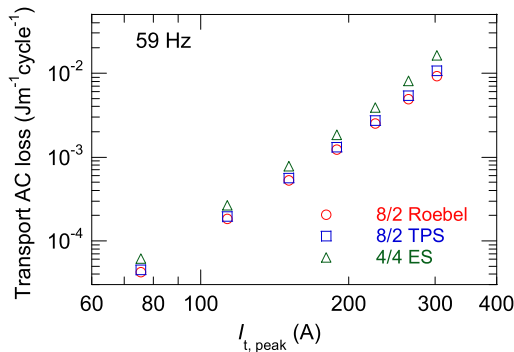

FIGURE 9. Comparison of transport AC loss in 8/2 Roebel cable, 8/2 TPS and 4/4 ES at 59 Hz.
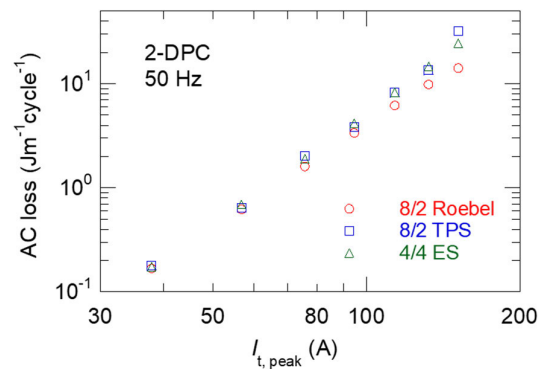

FIGURE 10. Comparison of AC loss values in 2-DPC coil winding comprised of the 8/2 Roebel, 8/2 TPS and 4/4 ES.

the existence of the horizontal gap [26], [37]. At $I_{t, peak} = 151$ A and 302 A, AC loss in 4/4 ES is 1.47 times and 1.76 times of that in the 8/2 Roebel cable, respectively.

V. RESULTS ANALYSIS: 2-DPC COIL WINDING
A. AC LOSS IN 2-DPC COIL WINDING
Figure 10 presents a comparison of the simulated AC loss values in the 2-DPC coil windings wound with the 8/2 Roebel cable, 8/2 TPS, and 4/4 ES and plotted as a function of the coil current amplitude. There is nearly no difference in AC loss values in the coil windings wound with different cables when the coil current is less than 60 A. The difference in the AC loss values between the coil windings wound with the 8/2 Robel cable and those wound with the 8/2 TPS and 4/4 ES becomes greater at high current amplitudes. We attribute the lower AC loss of the Roebel coil winding to the equal current sharing capability. In contrast, the 2-DPC coil winding wound with the 8/2 TPS generates the highest AC loss for all current amplitudes. The AC loss value in the 2-DPC winding wound with the 8/2 TPS is 2.3 times of that wound with the 8/2 Roebel cable at 151 A.

Figures 11 shows the normalised current density distribution, J/J_c in the 2-DPC coil windings wound with the 8/2

Roebel cable and 8/2 TPS, respectively, at $I_t = 113.4$ A. As a result of the equal current sharing between strands, the 2-DPC coil winding wound with the 8/2 Roebel cable is equivalent to a 4-DPC coil winding wound with 2 mm strands. In Figure 11(a), we could observe shielding currents (magnetization currents) in the two end coil discs that shield the radial magnetic field component in the end part of the coil winding [19], [36]. The fully penetrated region where $|J/J_c| > 1$ is the greatest for the outermost disc and the smallest for the innermost disc. There is un-penetrated or subcritical region even in the outermost disc. In contrast, current in the end pancake coil of the 8/2 TPS is mostly concentrated in the outermost disc and there is almost no shielding current. The induced shielding current for the bottom half of the pancake coil (blue colour) is almost the same as the transport current (red colour), which implies the net current for the bottom half of the PC is almost zero. The inner PC shows similar behaviour as the upper PC although its upper half of the PC does not contain any shielding current. These observations clearly indicate highly unequal current distribution of the coil winding wound with the 8/2 TPS. This behaviour causes high AC loss and hence the 8/2 TPS is not a favourable option for high-current applications.
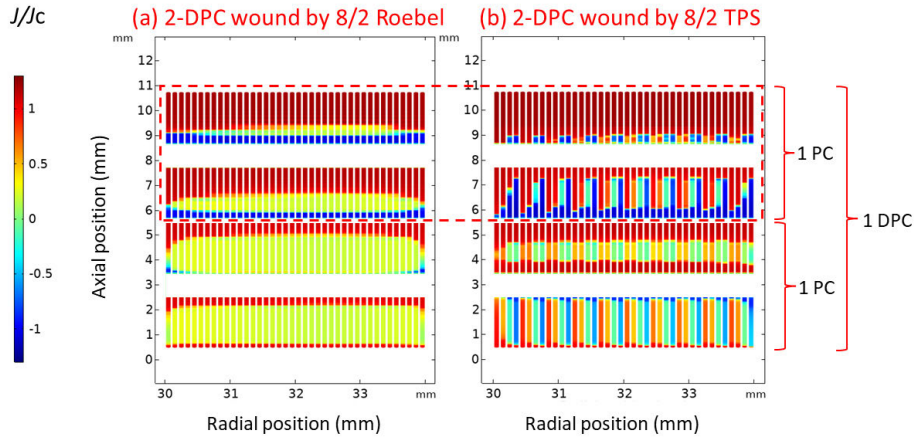
FIGURE 11. *J* distribution for 2-DPC coil windings wound with the 8/2 Roebel and 8/2 TPS at I_t = 113 A (I_t/I_{c0} = 0.3).
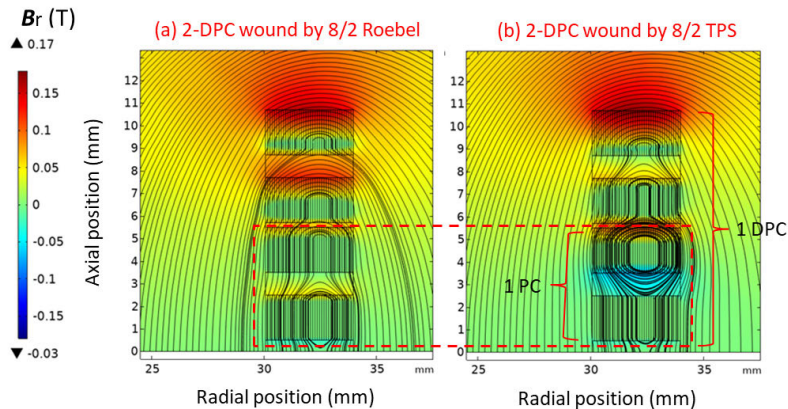

FIGURE 12. Radial magnetic field distribution around 2-DPC coil windings wound with the 8/2 Roebel and 8/2 TPS at 113.4 A.
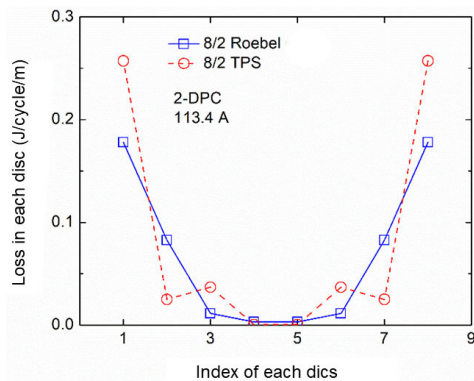

FIGURE 13. Loss density distribution in the 2-DPC coil windings wound with the 8/2 Roebel and 8/2 TPS (Each disc is half PC).

Figures 12 plots and compares the radial magnetic field component, B_r, distribution and the flux streamlines around the 2-DPC coil windings wound with the 8/2 Roebel cable and 8/2 TPS, respectively, at I_t = 113.4 A. The area filled with large B_r in the outermost disc of the 2 DPC coil winding wound with the 8/2 TPS is much greater than that of the 8/2 Roebel cable, while the area filled with large B_r in the second disc of the 2-DPC coil winding is smaller than that of the 8/2

Roebel cable. Another interesting phenomenon is appearance of closed-loop flux lines in the 3rd disc of the 2-DPC coil winding wound by the 8/2 TPS. The area with large B_r in the 3rd disc in the 2-DPC coil winding wound with the 8/2 TPS is much greater than that wound with the 8/2 Roebel cable. The magnetic field distributions in the coil windings are consistent with the current density distribution in figure 11.

Loss distributions of each disc (each half PC) in the 2-DPC coil windings wound with the 8/2 Roebel cable and 8/2 TPS at I_t = 113.4 A are compared in figure 13. The AC loss values in the discs #1 (or #8) and #3 (or # 6) in the coil winding wound with the 8/2 TPS are greater than those wound with the 8/2 Roebel cable while the AC loss values in the disc #2 (or #7) wound with the 8/2 TPS are smaller than those wound with the Roebel cable. The discs #1 (or #8) and #3 (or # 6) in the coil winding wound with the 8/2 TPS correspond to the parts where high current concentration is occurring as shown in figure 11 and this current concentration leads to high loss values in the discs.

B. AC LOSS IN 8-DPC COIL WINDINGS

Figures 14(a) and (b) show the current density distribution in the 8-DPC coil windings wound with the 8/2 Roebel cable and 8/2 TPS, respectively, at I_t = 113.4 A. As shown in
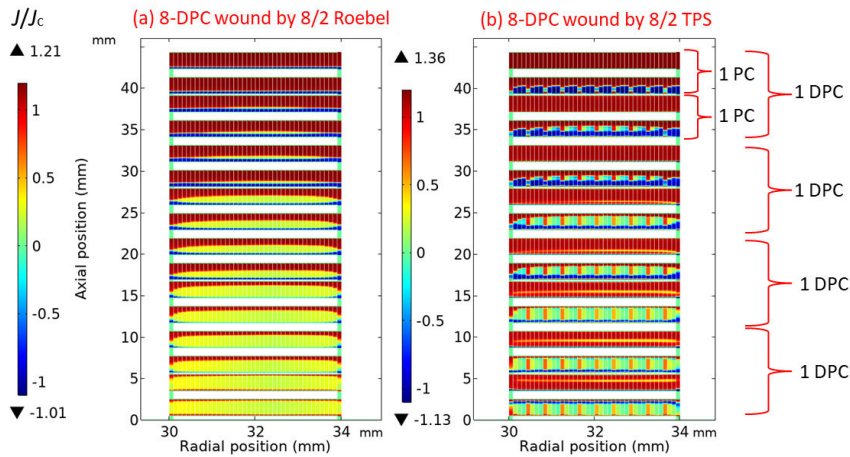
FIGURE 14. *J* distribution for 8-DPC coil windings wound with (a) 8/2 Roebel and (b) 8/2 TPS at 113.4 A ($I_t/I_{c0} = 0.3$).
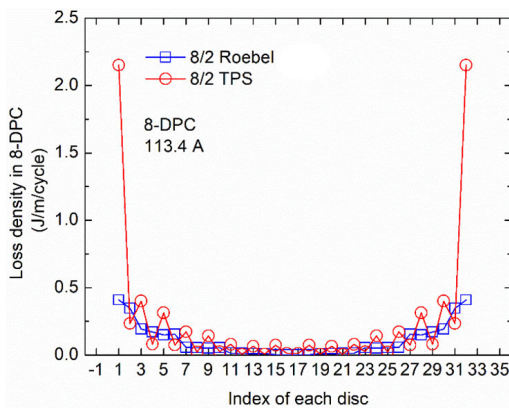

FIGURE 15. Loss density distribution in the 8-DPC windings wound with the 8/2 Roebel and 8/2 TPS.
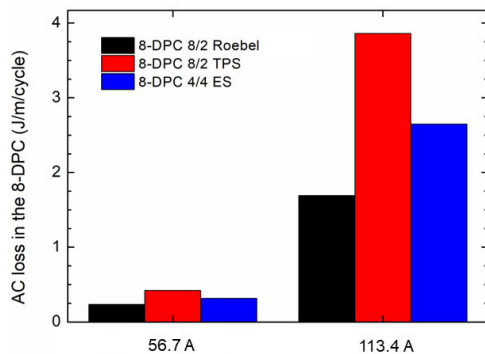

FIGURE 16. Comparison of AC loss values in the 8-DPC winding, wound with the 8/2 Roebel, 8/2 TPS and 4/4 ES, respectively.

figure 15(a), transport current flows at the outer edge of each disc for the 8-DPC winding wound with the 8/2 Reobel cable, while magnetization current is observed in each disc excluding the central disc due to symmetry to shield the radial magnetic field component in the end part of the coil winding, similar to figure 11(a). Unlike the 8-DPC coil winding wound with the 8/2 Roebel cable, the transport current is completely concentrated in the outer disc of each PC in the 8-DPC coil winding wound with the 8/2 TPS, and the inner disc of each PC carries no net current similar to the 2-DPC coil winding

case. In addition, $|J/J_c| > 1$ region is more focused in the end part of the coil winding where high AC loss is generated. The result shows that strong unequal current-sharing occurs in the entire 8-DPC coil winding wound with the 8/2 TPS and this, in turn, leads to high loss generation.

Loss distributions in each disc of the 8-DPC coil windings wound with the 8/2 Roebel cable and 8/2 TPS are compared in figure 15, when $I_t = 113.4$ A. The AC loss value in the end disc wound with the 8/2 TPS is nearly 5 times of that wound with the 8/2 Roebel cable. The zig-zag shaped loss distribution for the coil winding wound with the 8/2 TPS is due to strong unequal current distribution in the 8/2 TPS strands: high AC loss values correspond to high current concentration and low loss values correspond to low net current flow.

Figure 16 compares the AC loss values in the 8-DPC coil windings wound with the 8/2 Roebel, 8/2 TPS and 4/4 ES at $I_t = 56.7$ A and 113.4 A. The 8-DPC coil winding wound with the 8/2 Roebel cable has the smallest loss and the coil winding wound with the 8/2 TPS has the greatest loss at both current amplitudes. At 113 A, loss value in the 8-DPC coil winding wound with the 8/2 TPS is 2.2 times of that wound with the 8/2 Roebel cable.

VI. CONCLUSION

A new numerical approach using the widely used *H*-formulation in COMSOL Multiphysics is both proposed and demonstrated that can achieve equal current sharing and free current sharing among multiple strands both in straight cables and coil windings. This was done using 2D FEM on three cable case studies, i) 8/2 (eight 2 mm-wide strands) Roebel cable, 8/2 Roebel ii) two parallel stacks (8/2 TPS) which have the same geometrical dimensions as the 8/2 Roebel cable, 8/2 TPS iii) an equivalent four-conductor stack comprising of four 4 mm-wide conductors, 4/4 ES, as well as the windings wound by them, namely the two, and eight stacks of double pancakes (DPCs) wound with these cables. The numerical model was validated by comparing the simulated transport AC loss results in the straight 8/2 Roebel cable with previously measured results.

An electric circuit has been used to explain the current sharing among different strands in the straight 8/2 Roebel cable and 8/2 TPS. The analytical formula can explain the unequal current-sharing among different strands, consistent with the results from the numerical model.

On the straight cable level, we observe nearly the same pattern of J/J_c distribution in "Outer conductor" and "Inner conductor" at $I_t/I_{c0} = 0.8$ in Roebel cable, and both conductors are not fully penetrated having a portion of sub-critical area. In contrast, the pattern of J/J_c distribution in TPS is remarkably different. $|J/J_c|$ value of the "Outer conductor" in TPS is greater than 1 across the conductor width whereas there is 1/3 of the conductor width has less than 1 for the "Inner conductor". In terms of AC losses, it is observed that for a given cable current, the straight 4/4 ES has the greatest loss while the 8/2 Roebel cable has the smallest loss among the three cable types due to the equal current sharing behaviour. The difference in the AC loss values between the cables becomes greater with increasing the amplitude of the cable current.

On the coil winding level, transport current flows at the outer edge of each disc for the 8-DPC winding wound with the 8/2 Reobel cable, while magnetization current is observed in each disc excluding the central disc. The transport current is completely concentrated in the outer disc of each PC in the 8-DPC coil winding wound with the 8/2 TPS, and the inner disc of each PC carries no net current similar to the 2-DPC coil winding case. The result shows that strong unequal current-sharing occurs in the entire 8-DPC coil winding wound with the 8/2 TPS and this, in turn, leads to high loss generation. AC loss value in the end disc wound with the 8/2 TPS is nearly 5 times of that wound with the 8/2 Roebel cable. A zig-zag shaped loss distribution was found for the coil winding wound with the 8/2 TPS due to strong unequal current distribution in the 8/2 TPS strands: high AC loss values correspond to high current concentration and low loss values correspond to low net current flow.

REFERENCES

[1] W. Song, Z. Jiang, M. Staines, R. A. Badcock, S. C. Wimbush, J. Fang, and J. Zhang, "Design of a single-phase 6.5 MVA/25 kV superconducting traction transformer for the Chinese fuxing high-speed train," *Int. J. Electr. Power Energy Syst.*, vol. 119, Jul. 2020, Art. no. 105956.

[2] Y. Ohtsubo, M. Iwakuma, S. Sato, K. Sakaki, A. Tomioka, T. Miyayama, M. Konno, H. Hayashi, H. Okamoto, Y. Gosho, T. Eguchi, T. Saitoh, T. Izumi, and Y. Shiohara, "Development of REBCO superconducting transformers with a current limiting function—Fabrication and tests of 6.9 kV-400 kVA transformers," *IEEE Trans. Appl. Supercond.*, vol. 25, no. 3, Jun. 2015, Art. no. 5500305.

[3] E. Pardo, M. Staines, Z. Jiang, and N. Glasson, "AC loss modelling and measurement of superconducting transformers with coated-conductor roebel-cable in low-voltage winding," *Superconductor Sci. Technol.*, vol. 28, no. 11, Nov. 2015, Art. no. 114008.

[4] M. Yazdani-Asrami, M. Staines, G. Sidorov, M. Davies, J. Bailey, N. Allpress, N. Glasson, and S. A. Gholamian, "Fault current limiting HTS transformer with extended fault withstand time," *Superconductor Sci. Technol.*, vol. 32, no. 3, Mar. 2019, Art. no. 035006.

[5] M. Yazdani-Asrami, S. Seyyedbarzegar, A. Sadeghi, W. T. B. de Sousa, and D. Kottonau, "High temperature superconducting cables and their performance against short circuit faults: Current development, challenges, solutions, and future trends," *Superconductor Sci. Technol.*, vol. 35, no. 8, Aug. 2022, Art. no. 083002.

[6] L. Bottura, C. Rosso, and M. Breschi, "A general model for thermal, hydraulic and electric analysis of superconducting cables," *Cryogenics*, vol. 40, nos. 8–10, pp. 617–626, Aug. 2000.

[7] F. Weng, M. Zhang, T. Lan, Y. Wang, and W. Yuan, "Fully superconducting machine for electric aircraft propulsion: Study of AC loss for HTS stator," *Superconductor Sci. Technol.*, vol. 33, no. 10, Oct. 2020, Art. no. 104002.

[8] S. You, S. S. Kalsi, M. D. Ainslie, R. A. Badcock, N. J. Long, and Z. Jiang, "Simulation of AC loss in the armature windings of a 100 kW all-HTS motor with various (RE)BCO conductor considerations," *IEEE Access*, vol. 9, pp. 130968–130980, 2021.

[9] X. Chen, H. Gou, Y. Chen, S. Jiang, M. Zhang, Z. Pang, and B. Shen, "Superconducting fault current limiter (SFCL) for a power electronic circuit: Experiment and numerical modelling," *Superconductor Sci. Technol.*, vol. 35, no. 4, Apr. 2022, Art. no. 045010.

[10] W. Song, X. Pei, J. Xi, and X. Zeng, "A novel helical superconducting fault current limiter for electric propulsion aircraft," *IEEE Trans. Transport. Electrific.*, vol. 7, no. 1, pp. 276–286, Mar. 2021.

[11] A. Morandi, B. Gholizad, and M. Fabbri, "Design and performance of a 1 MW-5 S high temperature superconductor magnetic energy storage system," *Superconductor Sci. Technol.*, vol. 29, no. 1, Jan. 2016, Art. no. 015014.

[12] A. Morandi, L. Trevisani, F. Negrini, P. L. Ribani, and M. Fabbri, "Feasibility of superconducting magnetic energy storage on board of ground vehicles with present state-of-the-art superconductors," *IEEE Trans. Appl. Supercond.*, vol. 22, no. 2, Apr. 2011, Art. no. 5700106.

[13] M. Yazdani-Asrami, M. Zhang, and W. Yuan, "Challenges for developing high temperature superconducting ring magnets for rotating electric machine applications in future electric aircrafts," *J. Magn. Magn. Mater.*, vol. 522, Mar. 2021, Art. no. 167543.

[14] H. Maeda and Y. Yanagisawa, "Recent developments in high-temperature superconducting magnet technology (review)," *IEEE Trans. Appl. Supercond.*, vol. 24, no. 3, Jun. 2013, Art. no. 4602412.

[15] N. J. Long, R. A. Badcock, K. Hamilton, A. Wright, Z. Jiang, and L. S. Lakshmi, "Development of YBCO Roebel cables for high current transport and low AC loss applications," *J. Phys., Conf. Ser.*, vol. 234, no. 2, Jun. 2010, Art. no. 022021.

[16] F. Grilli, S. P. Ashworth, and S. Stavrev, "Magnetization AC losses of stacks of YBCO coated conductors," *Phys. C, Supercond.*, vol. 434, no. 2, pp. 185–190, Feb. 2006.

[17] Z. Jiang, R. A. Badcock, N. J. Long, M. Staines, K. P. Thakur, L. S. Lakshmi, A. Wright, K. Hamilton, G. N. Sidorov, R. G. Buckley, N. Amemiya, and A. D. Caplin, "Transport AC loss characteristics of a nine strand YBCO Roebel cable," *Superconductor Sci. Technol.*, vol. 23, no. 2, Feb. 2010, Art. no. 025028.

[18] N. Amemiya, T. Tsukamoto, M. Nii, T. Komeda, T. Nakamura, and Z. Jiang, "Alternating current loss characteristics of a Roebel cable consisting of coated conductors and a three-dimensional structure," *Superconductor Sci. Technol.*, vol. 27, no. 3, Mar. 2014, Art. no. 035007.

[19] S. Terzieva, E. Pardo, F. Grilli, A. Drechsler, A. Kling, A. Kudymow, F. Gömöry, and W. Goldacker, "Transport and magnetization AC losses of Roebel assembled coated conductor cables: Measurements and calculations," *Superconductor Sci. Technol.*, vol. 23, no. 1, Jan. 2010, Art. no. 014023.

[20] W. Goldacker, F. Grilli, E. Pardo, A. Kario, S. I. Schlachter, and M. Vojenčiak, "Roebel cables from REBCO coated conductors: A one-century-old concept for the superconductivity of the future," *Superconductor Sci. Technol.*, vol. 27, no. 9, Sep. 2014, Art. no. 093001.

[21] M. Takayasu, L. Chiesa, L. Bromberg, and J. V. Minervini, "HTS twisted stacked-tape cable conductor," *Superconductor Sci. Technol.*, vol. 25, no. 1, Jan. 2012, Art. no. 014011.

[22] Z. Jiang, N. Amemiya, K. Kakimoto, Y. Iijima, T. Saitoh, and Y. Shiohara, "The dependence of AC loss characteristics on the space in stacked YBCO conductors," *Superconductor Sci. Technol.*, vol. 21, no. 1, Jan. 2008, Art. no. 015020.

[23] M. Iwakuma, M. Nigo, D. Inoue, N. Miyamoto, K. Funaki, Y. Iijima, T. Saitoh, Y. Yamada, T. Izumi, and Y. Shiohara, "Temperature scaling of AC loss in YBCO superconducting tapes fabricated by the IBAD-PLD technique," *Superconductor Sci. Technol.*, vol. 19, no. 4, pp. 350–358, Apr. 2006.

[24] W. Zhou, Z. Jiang, M. Staines, W. Song, C. W. Bumby, R. A. Badcock, N. Long, and J. Fang, "Magnetization loss in REBCO Roebel cables with varying strand numbers," *IEEE Trans. Appl. Supercond.*, vol. 28, no. 3, Apr. 2018, Art. no. 8200605.

[25] E. Pardo, F. Grilli, Y. Liu, S. Wolftädler, and T. Reis, "AC loss modeling in superconducting coils and motors with parallel tapes as conductor," *IEEE Trans. Appl. Supercond.*, vol. 29, no. 5, Aug. 2019, Art. no. 5202505.

[26] Z. Jiang, K. P. Thakur, N. J. Long, R. A. Badcock, and M. Staines, "Comparison of transport AC losses in an eight-strand YBCO Roebel cable and a four-tape YBCO stack," *Phys. C, Supercond. Appl.*, vol. 471, nos. 21–22, pp. 999–1002, Nov. 2011.

[27] X. Zhao et al., "Design, development, and testing of a 6.6 MVA HTS traction transformer for high-speed train applications," *Superconductor Sci. Technol.*, vol. 36, no. 8, Aug. 2023, Art. no. 085009.

[28] J.-H. Kim, C. H. Kim, V. Pothavajhala, and S. V. Pamidi, "Current sharing and redistribution in superconducting DC cable," *IEEE Trans. Appl. Supercond.*, vol. 23, no. 3, Jun. 2013, Art. no. 4801304.

[29] M. Staines, Z. Jiang, N. Glasson, R. Buckley, and M. Pannu, "High-temperature superconducting (HTS) transformers for power grid applications," in *Superconductors in the Power Grid*. Amsterdam, The Netherlands: Elsevier, 2015, pp. 367–397.

[30] M. Yazdani-Asrami, M. Taghipour-Gorjikolaie, W. Song, M. Zhang, and W. Yuan, "Prediction of nonsinusoidal AC loss of superconducting tapes using artificial intelligence-based models," *IEEE Access*, vol. 8, pp. 207287–207297, 2020.

[31] W. Song, Z. Jiang, M. Staines, R. A. Badcock, and J. Fang, "Experimental and numerical transport AC losses in a four-strand Roebel cable bifilar stack," *Superconductor Sci. Technol.*, vol. 31, no. 11, Nov. 2018, Art. no. 115001.

[32] Z. Hong, A. M. Campbell, and T. A. Coombs, "Numerical solution of critical state in superconductivity by finite element software," *Superconductor Sci. Technol.*, vol. 19, no. 12, pp. 1246–1252, Dec. 2006.

[33] V. M. Rodriguez-Zermeno, N. Mijatovic, C. Traeholt, T. Zirngibl, E. Seiler, A. B. Abrahamsen, N. F. Pedersen, and M. P. Sorensen, "Towards faster FEM simulation of thin film superconductors: A multiscale approach," *IEEE Trans. Appl. Supercond.*, vol. 21, no. 3, pp. 3273–3276, Jun. 2010.

[34] B. Shen, F. Grilli, and T. Coombs, "Review of the AC loss computation for HTS using H formulation," *Superconductor Sci. Technol.*, vol. 33, no. 3, Mar. 2020, Art. no. 033002.

[35] M. Yazdani-Asrami, W. Song, X. Pei, M. Zhang, and W. Yuan, "AC loss characterization of HTS pancake and solenoid coils carrying nonsinusoidal currents," *IEEE Trans. Appl. Supercond.*, vol. 30, no. 5, Aug. 2020, Art. no. 5900709.

[36] W. Song, Z. Jiang, X. Zhang, M. Staines, R. A. Badcock, J. Fang, Y. Sogabe, and N. Amemiya, "AC loss simulation in a HTS 3-phase 1 MVA transformer using H formulation," *Cryogenics*, vol. 94, pp. 14–21, Sep. 2018.

[37] Z. Jiang, M. Staines, N. J. Long, R. A. Badcock, C. Bumby, E. Talantsev, K. Hamilton, R. G. Buckley, and N. Amemiya, "The scaling of transport AC losses in Roebel cables with varying strand parameters," *Superconductor Sci. Technol.*, vol. 27, no. 7, Jul. 2014, Art. no. 075007.

RODNEY A. BADCOCK (Senior Member, IEEE) has 32 years of research experience in applied research and development covering manufacturing process monitoring and control, materials sensing, and superconducting systems. Since 2006, he has concentrated on superconducting machines development, production, and excitation and control with the Paihau-Robinson Research Institute, Victoria University of Wellington, Lower Hutt, New Zealand. He is currently the Institute Deputy Director, the Chief Engineer, and a Professor, and specializes in the management of complex engineering projects, including customer-focused multidisciplinary programs. He is particularly known for the development of the superconducting dynamos for electric machines and the NZ MBIE program developing aircraft superconducting electric propulsion technology. He is recognized as one of the leading experts in the application of superconducting dynamos, cables, and protection to electric machines and translating high-temperature superconductivity into commercial practice that has included general cable superconductors, Siemens, HTS-110, and several compact fusion programs. Committed to the next generation, the Ph.D. students have gone on to achieve significant commercial success in their own right. He was awarded the 2022 Royal Society Te Aparangi Pickering Medal for developing superconducting technologies that enable electrical machines at the leading edge of current engineering practice. He was a Key Member of the team awarded the Royal Society of New Zealand Cooper Medal, in 2008, for the development of high-temperature superconducting cables for power system applications, including 1-MVA transformer, 60-MW hydro generator, and 150-MW utility generator.

NICHOLAS J. LONG (Senior Member, IEEE) received the M.Sc. degree in physics from Victoria University, and the Ph.D. degree in physics from the University of Southern California. From 1994 to 2013, he was with Industrial Research Ltd. (IRL). He is currently a Professor and the Director of the Robinson Research Institute, Victoria University of Wellington, New Zealand. He was the Founder of the program with IRL to develop HTS Roebel cables. His other HTS work has focused on enhancing wire performance and understanding the phenomenology of critical currents. More recent projects involve the application of superconductivity to satellite and space technology. His primary research interest includes high temperature superconductivity (HTS).


ZHENAN JIANG (Senior Member, IEEE) received the B.Eng. degree in electrical engineering from Chongqing University, Chongqing, China, in 1994, and the M.Eng. and Ph.D. degrees in applied superconductivity from Yokohama National University, Yokohama, Japan, in 2002 and 2005, respectively.

He was a Postdoctoral Research Fellow with Yokohama National University, from 2005 to 2008. He joined the Superconductivity Group currently known as the Robinson Research Institute, Victoria University of Wellington, New Zealand, in 2008, as a Research Scientist. He has a strong track record in the characterization of high-temperature superconductors (HTS), especially in AC loss. He is currently the principal scientist in the institute and leading AC loss research in the institute. His recent research interests include AC loss characterization in HTS, HTS applications, including transformers, flux pumps, magnets, and rotating machines.

Dr. Jiang has been awarded twice the Japan Society for the Promotion of Science (JSPS) Invitation Fellowship from Kyoto University, in 2011 and 2015, respectively. Since 2021, he has been an Editorial Board Member of *Superconductivity* (Elsevier). He was awarded the 2021 Scott Medal from Royal Society New Zealand for the work on measuring and modeling the response of superconductors.
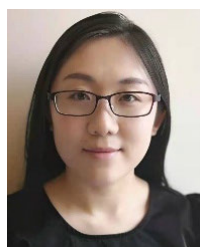
WENJUAN SONG (Member, IEEE) received the M.Eng. and Ph.D. degrees in electrical engineering from Beijing Jiaotong University, Beijing, China, in 2015 and 2019, respectively.

From 2016 to 2018, she was a Research Assistant with the Robinson Research Institute, Victoria University of Wellington, Wellington, New Zealand, for more than two years. From 2019 to 2021, she was a Postdoctoral Research Associate with the Department of Electronic and Electrical Engineering, University of Bath, Bath, U.K. Since 2022, she has been a Lecturer in electrically powered aircraft and operations with the Propulsion, Electrification and Superconductivity Theme/Group, Autonomous System and Connectivity Division, School of Engineering, University of Glasgow, Glasgow, U.K. Her research interests include protection solutions for electrically powered aircraft propulsion systems, research and development of high efficiency, and low loss superconducting applications, including superconducting fault current limiters, superconducting propulsion units, superconducting transformers, and artificial intelligence for superconducting components in modern cryo-electric aircraft.

● ● ●